

# PHYSICAL REVIEW B

## CONDENSED MATTER

THIRD SERIES, VOLUME 38, NUMBER 13

1 NOVEMBER 1988

### Optical and electron paramagnetic resonance studies of Fe impurities in yttrium aluminum garnet crystals

C. Y. Chen,<sup>\*†</sup> G. J. Pogatshnik,<sup>\*</sup> and Y. Chen

*Solid State Division, Oak Ridge National Laboratory, Oak Ridge, Tennessee 37831*

M. R. Kokta

*Union Carbide Corporation, Washougal, Washington 98671*

(Received 15 March 1988)

Optical-absorption and electron paramagnetic resonance (EPR) techniques were used to study iron impurities in yttrium aluminum garnet (YAG) crystals. Due to its low symmetry, YAG containing  $\text{Fe}^{3+}$  exhibited many EPR lines.  $\text{Fe}^{3+}$  ions in octahedral and tetrahedral sites were identified. A correlation study involving both EPR and optical-absorption measurements indicated that the absorption band at 255 nm, which had been previously attributed to an  $\text{Fe}^{3+}$  charge-transfer band, was a composite charge-transfer band made up of contributions from substitutional  $\text{Fe}^{3+}$  at both symmetry sites. Oxidation and reduction experiments up to 1700 K were performed. The former increased the  $\text{Fe}^{3+}$  concentration, and the latter diminished it. Conversion of  $\text{Fe}^{2+}$  to  $\text{Fe}^{3+}$  was governed by a thermal activation energy of  $3.0 \pm 0.3$  eV.

#### I. INTRODUCTION

Because of its technological importance as a solid-state laser host, single crystals of yttrium aluminum garnet, ( $\text{Y}_3\text{Al}_5\text{O}_{12}$  or YAG), have been investigated for more than two decades. Improvements in crystal growth technique developed for Nd:YAG laser rods have resulted in the production of very pure YAG crystals. Many of the trace impurities in the crystals cannot be detected in the absorption spectra of YAG. However, iron impurities do contribute to the optical absorption near the band edge and influence the uv optical properties of the material. The optical transitions which produce a broad absorption band at 255 nm result from charge transfer transitions from neighboring oxygen ligands to the empty orbitals of  $\text{Fe}^{3+}$  impurities.<sup>1</sup> Unlike the parity forbidden transitions between states in the  $3d$  manifold, the charge-transfer transitions are dipole allowed so the impurities can be easily detected in absorption spectroscopy. Transitions on  $\text{Fe}^{3+}$  ions also are the dominant features in room-temperature electron paramagnetic resonance spectra. Since iron impurities can be quenching sites for luminescence in laser materials, we have utilized both optical and magnetic resonance techniques to further characterize iron impurities in YAG.

In the YAG lattice aluminum ions occupy both octahedrally and tetrahedrally coordinated sites with 40% of the aluminum at octahedral sites and the remainder at

tetrahedral sites. Iron impurities substitute for aluminum sites in the YAG lattice. The optical absorption bands of iron in YAG have been determined by doping iron in YAG in concentrations of approximately 1 at.%.<sup>2</sup> In general, substitution of  $\text{Fe}^{3+}$  ions at the two types of aluminum sites should result in two sets of iron charge transfer absorption bands. However, only a single absorption band at 255 nm has been identified as a charge transfer transition. Meil'man *et al.* have suggested that the 255-nm absorption band is a composite which results from the overlap of the charge-transfer bands from the two different sites.<sup>3</sup> Masumoto and Kuwamo have also suggested that the 255-nm absorption band consists of more than one absorption center, based on their results of absorption measurements of crystals annealed under different partial pressures of oxygen.<sup>4</sup> Arsen'ev and Sviridov found no charge-transfer band between 255 and 370 nm. The results of the optical studies can be interpreted in several ways: The 255-nm absorption band is a composite of charge-transfer transitions of  $\text{Fe}^{3+}$  at octahedral and tetrahedral sites; the second set of charge-transfer bands may lie at higher energy than 255 nm; or Fe impurities occupy only one type of aluminum site in YAG. By identifying the  $\text{Fe}^{3+}$  EPR spectra for both octahedrally and tetrahedrally coordinated sites, and correlating changes in the EPR spectrum to optical absorption, we have been able to show that the 255-nm absorption band is due to composite charge-transfer bands from octahedral and tetrahedral sites.

## II. EXPERIMENTAL PROCEDURE

The nominally pure YAG crystals used in this work were obtained from the Allied Corporation. The samples were  $2.7 \pm 0.1$ -mm-thick plates with the [111] direction perpendicular to the crystal face. Analysis of the samples performed at the Oak Ridge National Laboratory using spark flame spectroscopy indicated the presence of impurities of Fe, Si, Mg, and Cr in concentrations of approximately 10 ppm. In addition, an iron-doped YAG crystal containing approximately 0.3 at. % Fe was provided by Union Carbide. The optical absorption measurements were made with a Perkin-Elmer Lambda-9 Spectrophotometer. Excitation and emission spectra were measured using a Spex Fluorolog 212 spectrofluorimeter. The emission was detected using a cooled Hamamatsu R928 photomultiplier tube. Excitation spectra were normalized to the incident light intensity by reference to a Rhodamine B dye solution. Magnetic resonance spectra at X band were obtained using a Varian EPR spectrometer with a maximum field of 12 kG. High-temperature heat treatments were performed using an Astro-Furnace with a graphite heating element. When used in conjunction with an alumina tube, heat treatments up to 1925 K, with an estimated accuracy of 15 K, could be obtained. Oxidation of the samples used flowing oxygen with the sample resting in a quartz or alumina tube. Reduction was accomplished by enclosing the sample in graphite with flowing nitrogen gas.

## III. EXPERIMENTAL RESULTS AND DISCUSSION

### A. Oxidation

Previous investigations have shown that the 255-nm (4.8 eV) absorption band can be greatly enhanced by oxidation.<sup>5</sup> This indicates that substantial amounts of iron impurities in YAG are present as  $\text{Fe}^{2+}$  ions in the as-grown state. Under oxidation, the valence states of the iron impurities can be switched from divalent to trivalent with a concomitant increase in the  $\text{Fe}^{3+}$  charge-transfer bands. The strength of the iron charge-transfer band can be correlated with the intensities of the paramagnetic  $\text{Fe}^{3+}$  lines after various annealing treatments.

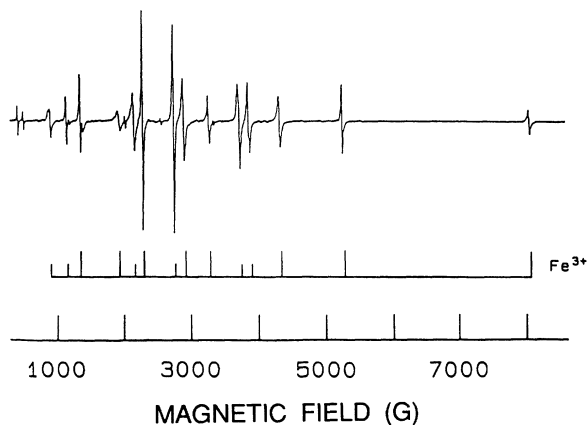


FIG. 1. EPR spectrum of an Fe-doped YAG sample at room temperature.

### 1. EPR

The samples for both EPR and optical spectroscopy were cut to dimensions of  $5 \times 2 \times 1$  mm<sup>3</sup> on x-ray oriented samples. The EPR spectra were taken by aligning the sample with the microwave field along the [110] axis, and with the magnetic field parallel to the [111] axis and perpendicular to the [110] axis. The EPR spectrum of a 1% iron-doped YAG sample is shown in Fig. 1, as an aid in the identification of the  $\text{Fe}^{3+}$  magnetic resonances. Because of the low site symmetry at the aluminum sites in YAG, the EPR spectrum of the  $\text{Fe}^{3+}$  ions is exceedingly rich. The  $\text{Fe}^{3+}$  lines are spread over a range of approximately 7000 G. Under oxidation and reduction, the changes in the relative intensities of the EPR lines indicate that two distinct sets of  $\text{Fe}^{3+}$  lines can be identified. The EPR spectra for  $\text{Fe}^{3+}$  in YAG in the as-grown state, as well as after reduction at 900 and 1500 K, is shown in Fig. 2. These spectra are highly sensitive to the orientation of the crystal; the crystal must be aligned to better than  $0.2^\circ$  along the [110] axis. Under oxidation of the sample at 900 K, the set of lines designated by the short marker lines at the bottom of the figure was diminished while the intensity of the other set (illustrated by the long marker lines) increased. We identify the magnetic reso-

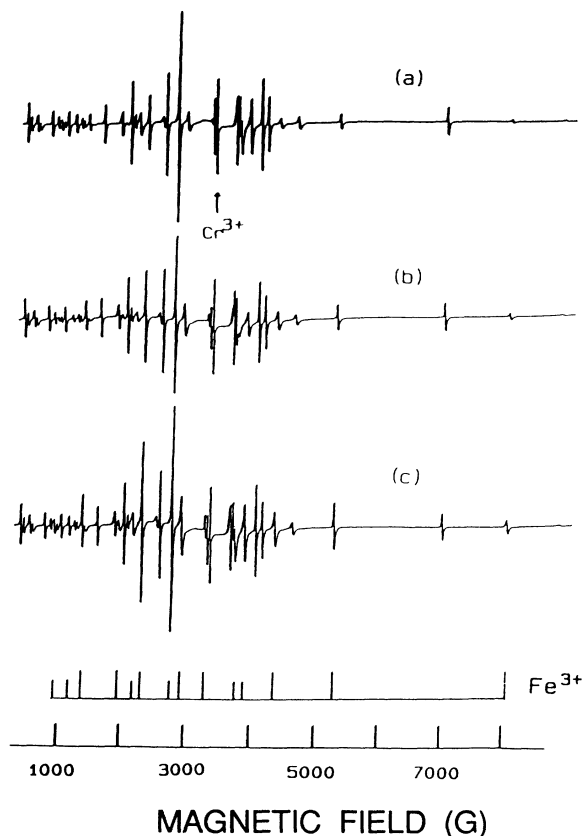


FIG. 2. EPR spectra of a YAG crystal aligned along the [110] axis with  $\mathbf{H}$  parallel to the [111] axis (a) in the as-grown state, (b) oxidized at 900 K, and (c) oxidized at 1500 K for 30 min. The stick diagram at the bottom illustrates the two different symmetry sites.

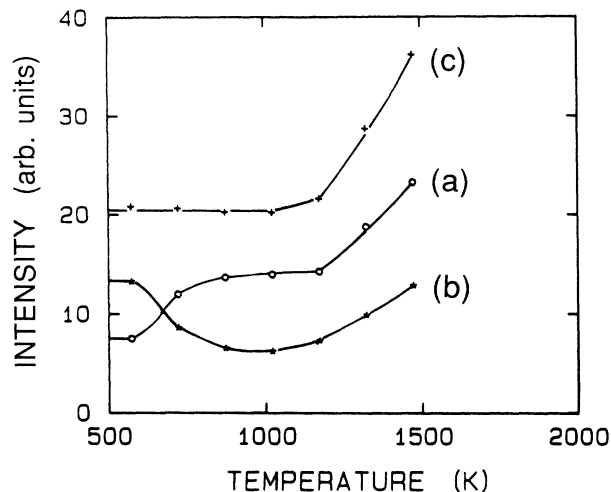


FIG. 3. Intensities of the  $\text{Fe}^{3+}$  resonances as a function of the annealing temperature in an oxidizing atmosphere for the (a) octahedral and (b) tetrahedral sites. Curve (c) represents the sum of the signals from the two symmetry sites.

nances of the two sets of lines indicated by the long and short markers as octahedrally and tetrahedrally coordinated  $\text{Fe}^{3+}$  ions, respectively. The assignment is based on the larger splitting of the magnetic resonances at the octahedral sites. This is consistent with the stronger crystal field at octahedral sites as determined by optical transitions of Fe-doped YAG.<sup>3,6</sup>

Figure 3 illustrates the behavior of the intensities of the  $\text{Fe}^{3+}$  resonances as a function of temperature for the octahedral and tetrahedral sites, labeled as (a) and (b), respectively. Typical error bars are illustrated in the figure. Curve (c) represents the summation of the resonance signals from the two different symmetry sites. The simple summation procedure can be justified on the basis of the similarity in the linewidths and relaxation times, as determined by the temperature dependence of the EPR signals, for the  $\text{Fe}^{3+}$  ions at the two distinct sites. We can divide the data into three temperature regions: Region I covers 300 to 600 K, region II from 600 to 1100 K, and region III for  $T > 1100$  K. In region I, oxidation for  $T < 600$  K shows no significant change from the as-grown crystals. In region II (600 to 1100 K) there is a decrease in intensity of the tetrahedral  $\text{Fe}^{3+}$  resonances and an increase in that at octahedral sites. In a subsequent section we will show that this preferential population of octahedrally coordinated  $\text{Fe}^{3+}$  occurs in reverse over the same temperature range under reducing conditions. Therefore the interchange of intensities between the alternate sites is a thermally activated process which is independent of the annealing atmosphere. At temperatures above 1100 K, the intensities of both sets of lines increase.

## 2. Optical absorption

Changes in the optical absorption in the YAG crystals can be correlated with the observed differences in the EPR spectra. The optical absorption spectrum of a 2.7-mm-thick YAG crystal, before and after oxidation, is

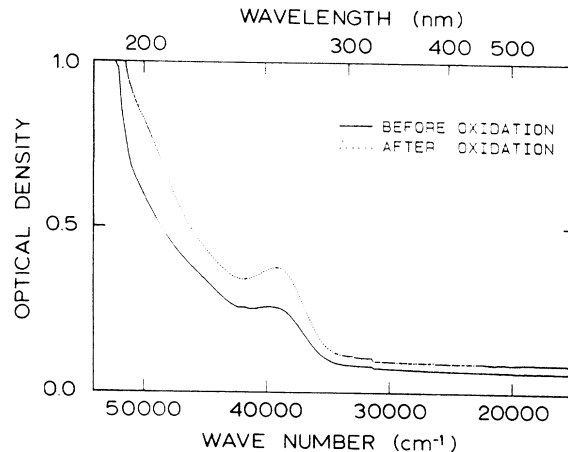


FIG. 4. The optical absorption spectrum of a YAG crystals (a) before, and (b) after oxidation at  $T = 1700$  K.

shown in Fig. 4. The  $\text{Fe}^{3+}$  charge-transfer band at 255 nm is the only prominent feature near the band edge. Oxidation above 1100 K results in a monotonic increase in the intensity of the charge-transfer band as illustrated in the figure. The growth of the 255-nm absorption band after 30 min oxidation is shown as a function of oxidation temperature in Fig. 5. The absorption coefficient at 255 nm remains essentially unchanged until temperatures above 1100 K. Above 1100 K there is an increase in the intensity of the charge-transfer band as the sample is oxidized at successively higher temperatures. The growth is due to an overall  $\text{Fe}^{2+} \rightarrow \text{Fe}^{3+}$  conversion under oxidation. The experiments were performed under somewhat different conditions. The samples were oxidized in two different tubes: an alumina tube which contained an abundance of Fe impurities, and a quartz tube which was essentially iron-free. The solid line in Fig. 5 corresponds to the 255-nm absorption for a sample oxidized in an alumina tube and the dashed line represents oxidation in a quartz tube. Previously, we have observed the diffusion

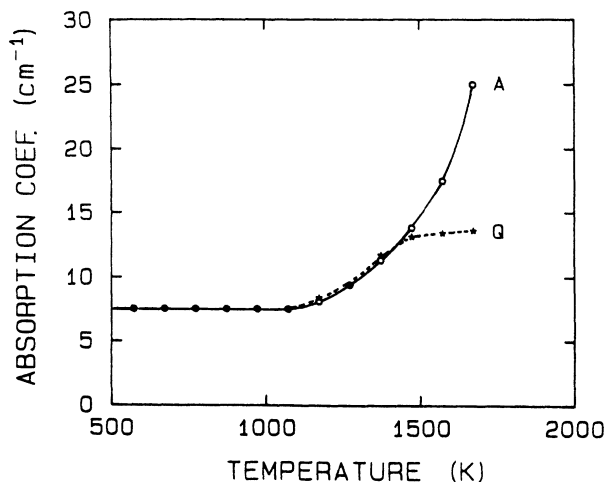


FIG. 5. The growth of the 255-nm absorption band versus isochronal heat treatment in an oxidizing atmosphere.

of Fe at  $T > 1600$  K into high-purity MgO samples during heat treatments in alumina tubes.<sup>7</sup> Therefore, we attributed the difference between the growth curves to diffusion of iron from the alumina tube into the sample. The increase in the absorption at 255 nm correlates well with the summation of the EPR line intensities of  $\text{Fe}^{3+}$  ions in the octahedral and tetrahedral sites as shown in Fig. 3(c). We observed no change in the 255-nm absorption band which could be attributed to a single type of  $\text{Fe}^{3+}$  site. The data indicates that the  $\text{Fe}^{3+}$  charge transfer bands at both symmetry sites overlap in the 255-nm spectral region.

The results shown in regions I and III of Fig. 3 provide a meaningful interpretation. In region I the temperatures are too low to cause appreciable ionic migration. In region III ( $T > 1100$  K), thermal agitation of ionic species is sufficiently large that long-range ionic migration began to take place. The optical data in Fig. 5 illustrates that the 255-nm band did not increase until 1100 K; above 1400 K the results depend on whether a quartz tube or alumina tube was used. The contrasting results of using an Fe-free and Fe-laden tube above 1400 K indicates that the excess Fe was derived from the alumina tube, and that long-range migration of Fe into the bulk sample was involved. The increase in absorption at 255-nm between 1100 and 1400 K, regardless of the iron content of the tube, indicates an overall increase in  $\text{Fe}^{3+}$  content at the expense of  $\text{Fe}^{2+}$  ions present in the crystal. One can deduce from the quartz tube results that there initially existed about as much  $\text{Fe}^{2+}$  as  $\text{Fe}^{3+}$ . The results in region II (600–1100 K), are less obvious. We interpret the increase of the octahedral  $\text{Fe}^{3+}$  and the decrease of tetrahedral  $\text{Fe}^{3+}$  as due to the short range thermal hopping of Fe impurities, and/or indigenous ions, independent of the ambient atmosphere.

One other observation should be noted. In Fig. 3 the EPR signals of the octahedral and tetrahedral  $\text{Fe}^{3+}$  ions increased and decreased by a factor of two respectively in region II, such that the sum of the intensities remained constant. In Fig. 5, it is noted that the optical absorption coefficient is also constant in the region. We did not observe appreciable changes in the half-width or peak wavelength of the 255-nm charge-transfer band. Therefore, we conclude that (1) both the tetrahedral and octahedral  $\text{Fe}^{3+}$  ions give rise to the charge transfer band at 255 nm, and (2) their oscillator strengths are comparable.

### 3. Activation energy

An estimate of the activation energy for the conversion of  $\text{Fe}^{2+}$  to  $\text{Fe}^{3+}$  under oxidation can be obtained by using the "cross-cut" method.<sup>8</sup> Samples of YAG were isothermally annealed in oxygen as a function of time at three different temperatures. Figure 6 is a plot of the absorbance at 255 nm versus the square root of the accumulated oxidation time at three different temperatures. The linear dependence versus  $t^{1/2}$  suggests that the rate-limiting process is one of diffusion. We have made the approximation of one-dimensional diffusion to simplify the analysis. The approximation is valid since the surface

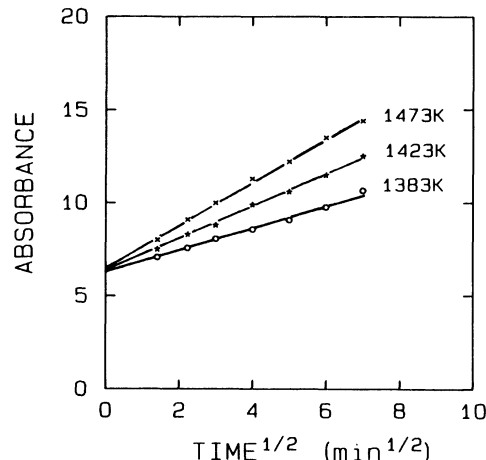


FIG. 6. The absorbance at 255 nm vs the square root of the accumulated oxidation time at three different temperatures.

area of the samples was much greater than the sample thickness. Under these assumptions, the absorption coefficient as a function of oxidation time and temperature is related by the expression

$$te^{-E/kT} = \text{const},$$

where  $t$  is the annealing time,  $T$  is the oxidation temperature, and  $E$  is the activation energy for the process. Figure 7 is a plot of the time versus  $T^{-1}$  for a constant absorption coefficient. The slope of the graph can be used to determine the activation energy. Over this temperature range of about 100 K, we obtained an activation energy of  $E = 3.0 \pm 0.3$  eV. This activation energy does not take into account the lower activation energy of the  $\text{Fe}^{3+}$  conversion between tetrahedral and octahedral sites in the temperature region from 600 to 1100 K as previously discussed.

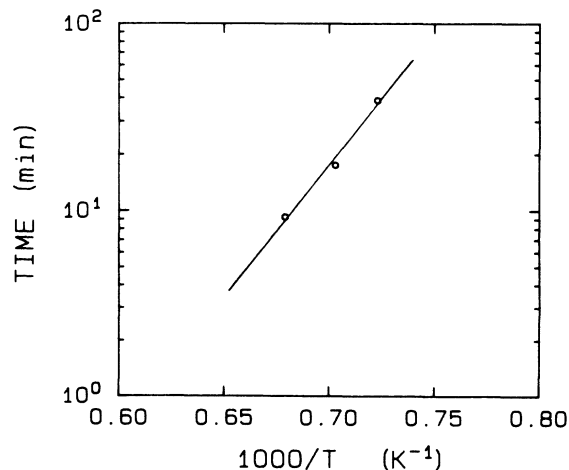


FIG. 7. Time of the oxidation vs  $T^{-1}$  for a constant absorbance.

### B. Reduction

To complement the oxidation experiments, we also studied the properties of  $\text{Fe}^{3+}$  in YAG under reducing conditions. The sample were reduced in graphite with flowing nitrogen gas for 30 min at each temperature. Figure 8 shows the behavior of the  $\text{Fe}^{3+}$  paramagnetic resonances at the octahedral and tetrahedral sites as a function of reduction temperature. As in the oxidation case, the data can be divided into three temperature ranges. From room temperature to 600 K there was no appreciable change in the magnetic resonance spectra. From 600 to 1100 K, we again observed the conversion of some  $\text{Fe}^{3+}$  ions between the two symmetry sites. As indicated in the previous section, this behavior was identical to the results under oxidation. Above 1100 K, the magnetic resonance lines from both  $\text{Fe}^{3+}$  sites decrease as the reduction temperature is increased. The decrease in the intensity of the  $\text{Fe}^{3+}$  lines is attributed to the  $\text{Fe}^{3+} \rightarrow \text{Fe}^{2+}$  reduction.

Figures 9(a) and (b) show the EPR spectra of an as-grown YAG sample before and after reduction for 30 min at 1500 K. After reduction, the magnetic resonance lines from  $\text{Fe}^{3+}$  and  $\text{Cr}^{3+}$  had decreased in intensity. In addition, Fig. 9(c) shows a new single line that increased in intensity at higher reduction temperatures. Figure 10 shows an expanded spectrum at room temperature of that line. The intensity of the line did not vary appreciably with angle. Measurements of the  $g$  values for the line parallel and perpendicular to the [111] crystal axis were made and values of  $g_{\parallel} = 1.9941 \pm 0.0005$  and  $g_{\perp} = 1.9939 \pm 0.0005$  were obtained. Although  $\Delta g = 0.0002$  is larger than the quoted uncertainties in the individual  $g$  values, nevertheless, we were able to detect a relative shift to higher field as the crystal was rotated perpendicular to the [111] axis. The room-temperature linewidth at 9.4 GHz was  $22 \pm 2$  G. A line similar to this

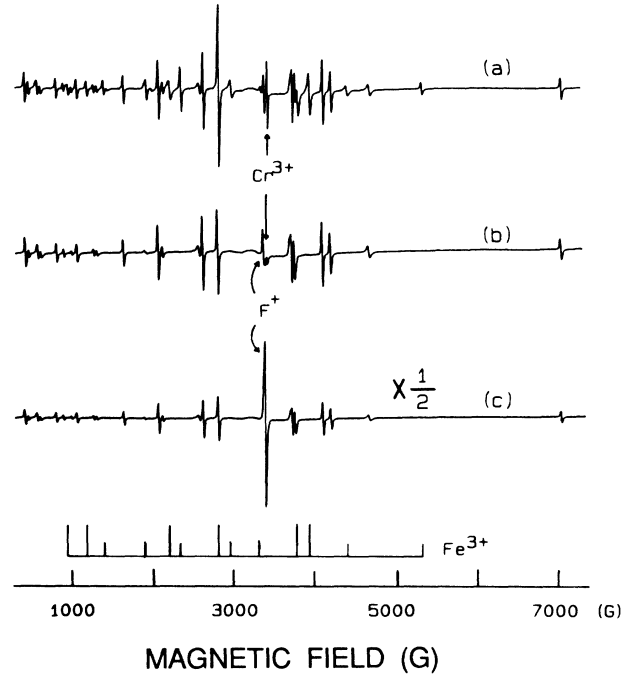


FIG. 9. EPR spectra of a YAG crystal aligned along the [110] axis with  $\mathbf{H}$  parallel to the [111] axis (a) in the as-grown state, (b) reduced at 1500 K, and (c) reduced at 1650 K for 30 min. Spectrum (c) illustrates a signal which was previously attributed to the  $F^+$  center.

had previously been reported by Mori<sup>9</sup> and Karaseva *et al.*<sup>10</sup> and was attributed to an unpaired electron trapped at an oxygen vacancy ( $F^+$  center), albeit the former author reported a line width of 34 G. The difference in linewidth may be due to differences in strain broadening of the EPR lines in the two different crystals. However, unlike most  $F^+$  centers, the signal from this center is not easily saturated with microwave power. We

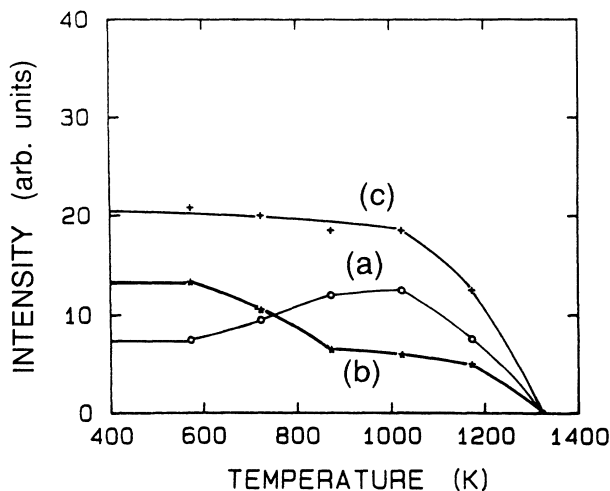


FIG. 8. Intensities of the  $\text{Fe}^{3+}$  resonances as a function of the annealing temperature in a reducing atmosphere for the (a) octahedral and (b) tetrahedral sites. Curve (c) represents the sum of the signals from the two symmetry sites.

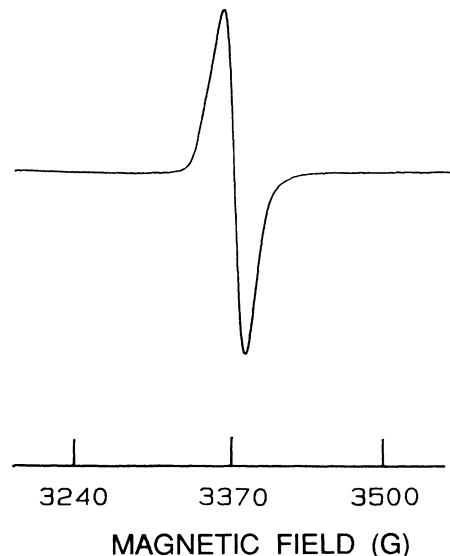


FIG. 10. An expanded spectrum of the EPR signal attributed to the  $F^+$  center.

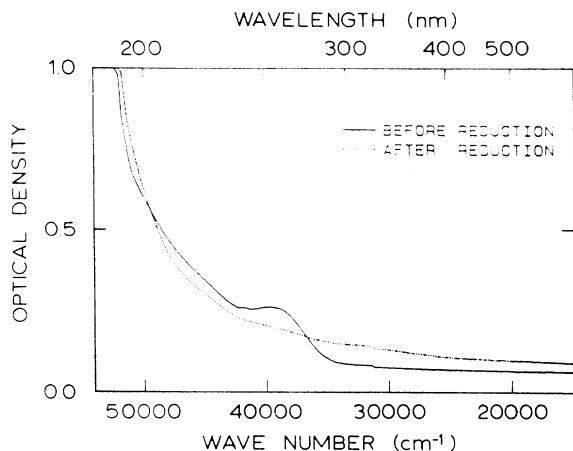


FIG. 11. The optical absorption spectrum of a YAG crystal (a) before, and (b) after reduction at  $T=1500$  K.

observed no saturation at room temperature although we were able to saturate the signal at high microwave powers at 77 K. Therefore, the spin-lattice relaxation time for this center in YAG is shorter than one would expect for the analogous  $F$  center in the alkali halides.

The optical absorption spectrum of a YAG crystal, before and after reduction, is shown in Fig. 11. At high reduction temperatures, ( $T > 1100$  K), the 255-nm absorption band decreases. Figure 12 shows the absorption coefficient at 255 nm as a function of reducing temperature. A comparison of Figs. 12 and 5 shows that the onset of  $\text{Fe}^{2+} \rightleftharpoons \text{Fe}^{3+}$  conversion takes place at 1100 K under oxidation and reduction. Again the absorbance at 255 nm is correlated with the sum of the EPR resonances from  $\text{Fe}^{3+}$  ions at octahedral and tetrahedral sites. The results from the reduction of iron in YAG also suggest that the 255-nm absorption band is a composite from iron impurities at the two different symmetry sites.

#### IV. SUMMARY AND CONCLUSIONS

Optical absorption and EPR techniques were used to study iron impurities in YAG. The room-temperature EPR spectra exhibited signals from  $\text{Cr}^{3+}$  and  $\text{Gd}^{3+}$ , as well as two sets of lines from  $\text{Fe}^{3+}$  impurities. One set of  $\text{Fe}^{3+}$  lines originates from  $\text{Fe}^{3+}$  ions substituting for  $\text{Al}^{3+}$  in the distorted octahedral sites, and the other set with a broader spectrum was from  $\text{Fe}^{3+}$  substituting for  $\text{Al}^{3+}$  ions at the distorted tetrahedral site.

The presence of  $\text{Fe}^{3+}$  in YAG results in a charge-transfer band which absorbs at 255 nm. The combination of paramagnetic and optical spectroscopy have shown that this absorption band in YAG is a composite charge-

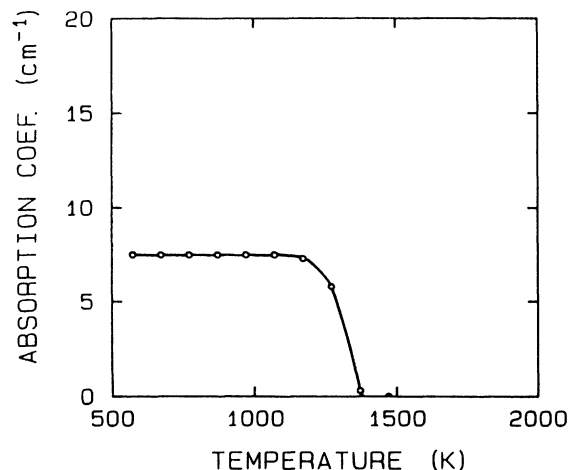


FIG. 12. The decay of the 255-nm absorption band vs isochronal heat treatment in a reducing atmosphere.

transfer band from  $\text{Fe}^{3+}$  ions at both octahedral and tetrahedral sites in the lattice. Furthermore, it is deduced that their oscillator strengths are comparable.

Studies in oxidation and reduction at elevated temperatures were performed using both EPR and optical absorption techniques. The  $\text{Fe}^{3+}$  concentration increased with oxidation and decreased with reduction. Conversion of  $\text{Fe}^{2+}$  to  $\text{Fe}^{3+}$  was governed by a thermally activated process with an energy of  $3.0 \pm 0.3$  eV. In a reducing atmosphere  $\text{Fe}^{3+}$  ions vanished at temperatures above 1400 K.

Results from thermal treatments in oxidizing and reducing atmospheres demonstrate that at  $T < 600$  K there exists no ionic migration. At temperatures between 600 and 1100 K, short-range migration of Fe impurities and/or the indigenous ions give rise to an increase of the octahedral  $\text{Fe}^{3+}$  signals, attended by a decrease of the tetrahedral  $\text{Fe}^{3+}$  ions, independent of the atmosphere. At  $T > 1100$  K, oxidation increases the  $\text{Fe}^{3+}$  signals at the expense of  $\text{Fe}^{2+}$  ions in the crystal, and reduction has the opposite effect.

#### ACKNOWLEDGMENTS

The authors wish to express their thanks to Marvin Abraham for his helpful suggestions and his assistance. We would also like to thank Larry Halliburton for the use of his experimental facilities. This research was sponsored by the Defense Advanced Research Projects Agency under Interagency Agreement 40-1611-85 with Martin Marietta Energy Systems, Inc., Contract No. DE-AC05-84OR21400 with the U.S. Department of Energy.

\*Also Dept. of Materials Engineering, North Carolina State University, Raleigh, NC 27695.

†Present address: Dept. of Physics, Oklahoma State University, Stillwater, OK 74078.

‡D. E. Lackison, G. B. Scott, and J. L. Page, Solid State Com-

mun. **14**, 861 (1974).

<sup>2</sup>P. A. Arsen'ev and D. T. Sviridov, Kristallografiya **14**, 687 (1969) [Sov. Phys.—Crystallogr. **14**, 578 (1970)].

<sup>3</sup>M. L. Meil'man, M. V. Korzhik, V. V. Kuz'min, M. G. Livshit, Kh. S. Bagdasarov, and A. M. Kevorkov, Dokl. Akad. Nauk

- SSSR **274**, 576 (1984) [Sov. Phys.—Dokl. **29**, 61 (1984)].
- <sup>4</sup>T. Masumoto and Y. Kuwano, Jpn. J. Appl. Phys. **24**, 546 (1985).
- <sup>5</sup>H. Haneda, Y. Miyazawa, and S. Shirasaki, J. Cryst. Growth **68**, 581 (1974).
- <sup>6</sup>P. Kohler and G. Amthauer, J. Solid State Chem. **28**, 329 (1979).
- <sup>7</sup>Y. Chen (unpublished).
- <sup>8</sup>J. Crank, *The Mathematics of Diffusion* (Clarendon, Oxford, 1956).
- <sup>9</sup>K. Mori, Phys. Status Solidi A **42**, 375 (1977).
- <sup>10</sup>L. G. Karaseva, N. Yu. Konstantinov, and V. V. Gromov, Radiat. Phys. Chem. **26**, 723 (1985).